Chimica Techno Acta
published by Ural Federal University
journal homepage: chimicatechnoacta.ru

ARTICLE
2021, vol. 8(1), № 20218108
DOI: 10.15826/chimtech.2021.8.1.08

Phase equilibria in the $YFeO_3$ – $YCoO_3$ system in air

A.V. Bryuzgina, A.S. Urusova*, I.L. Ivanov, V.A. Cherepanov

Institute of Natural Science and Mathematics, Ural Federal University,
Lenin av. 51, Yekaterinburg, 620000 Russia
* Corresponding author: Anastasia.Podzorova@urfu.ru

This article belongs to the regular issue.

Abstract

$YFe_{1-x}Co_xO_3$ solid solutions were prepared by glycerol-nitrate technique. The homogeneity range of solid solutions was studied within the temperature range 1173 – 1573 K. A continues series of solid solution below the decomposition temperature of $YCoO_3$, which was shown to be equal to 1266 ± 6 K, begins to narrow at higher temperatures and becomes equal to $0 \le x \le 0.1$ at 1573 K. The phase diagram of the $YFeO_3$ – $YCoO_3$ system in the "T – composition" coordinates was divided into three fields. Similar to the parent ternary oxides, all single-phase $YFe_{1-x}Co_xO_3$ solid solutions possess orthorhombically distorted perovskite structure (*Pnma* space group). Unusual behavior of orthorhombic distortions in $YFe_{1-x}Co_xO_3$ with temperature was explained by probable changes in spin state of Co^{3+} ions.

Keywords

solid solutions
perovskite crystal structure
phase diagram

Received: 14.03.2021
Revised: 10.04.2021
Accepted: 11.04.2021
Available online: 13.04.2021

1. Introduction

Yttrium ferrite and yttrium cobaltite with the perovskite structure and their mixed derivates attract much attention due to a set of electrical and magnetic properties [1-12]. Although their structural features and some functional properties were widely studied [1-16], there is lack information concerning phase equilibria and homogeneity ranges of $YFe_{1-x}Co_xO_3$ solid solutions. It is worth noting that phase equilibria in the Y – Fe – O system as well as thermodynamic characteristics of ternary oxides inside including $YFeO_3$ were studied in detail [17-21]. Also, detailed information available for the Fe – Co – O system [22-24]. Much less information can be found for the Y – Co – O system and the thermal stability of $YCoO_3$ [16, 25]. Thus, the aim of present work was determination of homogeneity ranges of $YFe_{1-x}Co_xO_3$ solid solutions as a function of temperature in air and establishing of phase equilibria in the $YFeO_3$ – $YCoO_3$ system.

2. Experimental

The samples were prepared via the glycerol-nitrate technique. The starting materials — Y_2O_3, metallic Co, $FeC_2O_4 \cdot 2H_2O$ — were dissolved in nitric acid and then glycerol was added. Metallic cobalt was prepared from Co_3O_4 by reduction in hydrogen flow at 923 K. The solution was carefully heated to dryness. The obtained residue was slowly heated up and annealed at 1173 K for 20 h. Final annealing of the samples were performed at required temperatures in air for 96 h with grinding after each 12 h. The samples were quenched to room temperature (RT) by removing them from a furnace and placing them to a cold massive copper plate. Phase identification was carried out by means of X-ray powder diffraction (XRD) using a Shimadzu XRD 7000 diffractometer (Cu Kα radiation, 2θ = 20°–90°, 0.02 deg/min, 5 s/point). High temperature XRD measurements were performed using a HTK 1200N (Anton Paar, Austria) high temperature chamber installed at the diffractometer. Unit cell parameters were calculated using Celref 3 software. The structure was refined by full-profile Rietveld analysis using Fullprof 2017 software.

TGA measurements were performed using a STA 409 PC instrument (Netzsch) within the temperature range of 300 – 1373 K in air.

3. Results and Discussion

First, the parent oxides of the studied system $YFeO_3$ and $YCoO_3$ were prepared and examined. Yttrium ferrite quenched from high temperature within the entire range (1173 – 1473 K) or slowly cooled to RT possesses orthorhombically distorted perovskite structure, which is in good agreement with the results reported earlier [1-4]. Fig. 1 illustrates XRD patterns of $YFeO_3$ prepared at various conditions and evaluated values of unit cell parameters, as an example. The XRD pattern refined by the Rietveld method and structural model of $YFeO_3$ designed

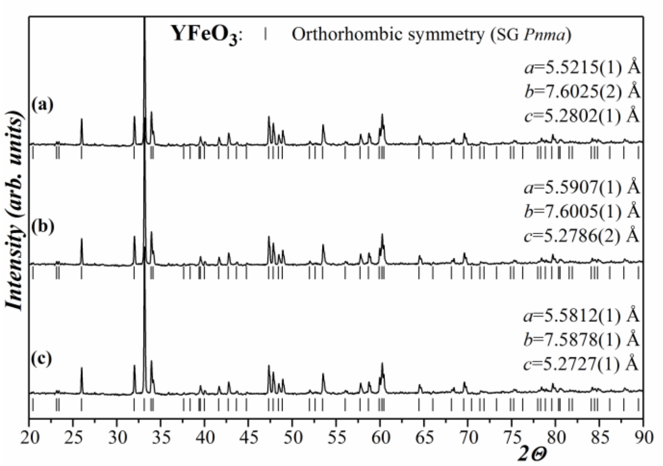

Fig. 1 XRD patterns of $YFeO_3$ quenched from various temperatures in air: (a) 1373 K; (b) 1173 K and (c) slowly cooled to room temperature and unit cell parameters evaluated by the Rietveld refinement

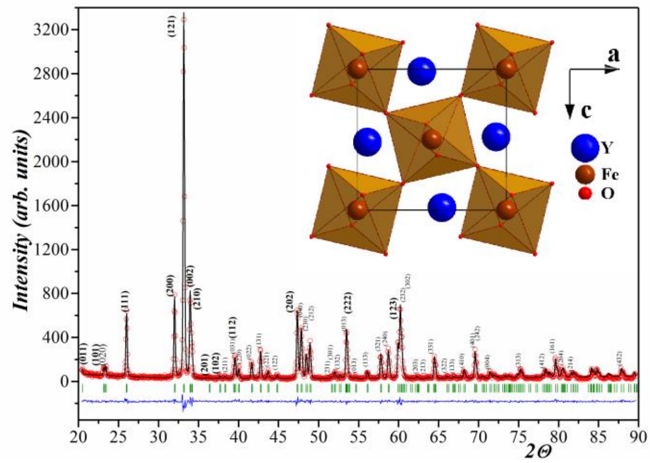

Fig. 2 XRD pattern refined by the Rietveld method and structural model of $YFeO_3$ along the *b* axis designed using the "Diamond 3.2" software.

using the "Diamond 3.2" software is shown in Fig. 2.

Single-phase yttrium cobaltite $YCoO_3$ was obtained only at relatively low temperatures 1173 and 1223 K. Like ferrite it possesses the orthorhombic structure (SG *Pnma*). The structural parameters of $YCoO_3$ quenched from 1173 and 1223 K refined by the Rietveld method are listed in Table 1.

To preliminarily estimate the decomposition temperature of $YCoO_3$, TGA measurements in a dynamic mode with a heating rate of 3.2 K/min were performed. A sharp drop in the mass of the sample was detected at 1300 K (Fig. 3).

Table 1 The structural parameters of $YCoO_3$ quenched from 1173 and 1223 K refined by the Rietveld method

SG *Pnma*: Y*(4c)*(x; 0.25; z); Co*(4a)*(0; 0; 0); O1*(4c)*(x; 0.25; z); O2*(8d)*(x; y; z)		
T, K	1173	1223
a, Å	5.41656(5)	5.41784(5)
b	7.36230(7)	7.36195(7)
c, Å	5.13591(5)	5.13604(5)
V, (Å)^3	204.811(1)	204.855(3)
x(Y)	0.4316(2)	0.4315(2)
z(Y)	0.0183(3)	0.0184(3)
x(O1)	0.5287(1)	0.5285(2)
z(O1)	0.5956(2)	0.5972(1)
x(O2)	0.2002(1)	0.1988(1)
y(O2)	0.0487(8)	0.0487(8)
z(O2)	0.3051(2)	0.3047(1)
$d_{(Y)-(O1)}$, Å	2.234(8)	2.227(7)
$d_{(Y)-(O2)}$, Å	2.437(6)	2.439(6)
$d_{(Y)-(O2)}$, Å	2.266(6)	2.263(6)
$d_{(Y)-(O2)}$, Å	2.558(6)	2.557(6)
$d_{(Co)-(O1)}$, Å	1.911(2)	1.913(2)
$d_{(Co)-(O2)}$, Å	1.939(6)	1.933(6)
$d_{(Co)-(O2)}$, Å	1.941(7)	1.949(6)
R_p, %	10.7	13.2
R_{wp}, %	12.3	15.5
R_{exp}, %	9.18	11.3
R_{Br}, %	3.58	3.10
R_f, %	6.85	3.11
χ^2	1.783	1.877

To refine the decomposition temperature in TGA measurements, a static mode was used. The following protocol was used: a single-phase sample was heated at a rate of 1 K/min to 1110 K and equilibrated at this temperature for 8 h. Then the temperature was increased in a step of 20 K and the sample was kept at a fixed temperature until a constant mass was established. No significant mass changes were detected at $T \leq 1260$ K. The next step to 1280 K results in a dramatic weight loss.

XRD analysis of the sample quenched after annealing at 1273 K, which was originally a single-phase $YCoO_3$, showed the presence of significant amounts of yttrium oxide and cobalt oxide (II) as secondary phases (Fig. 4). It should be mentioned that small amount of Co_3O_4 forms due to partial oxidation of CoO while cooling since latter is thermodynamic stable form of cobalt oxide at 1273 K in air.

Thus, one can conclude that $YCoO_3$ decomposes according the reaction

$$YCoO_3 = ½\,Y_2O_3 + CoO + ¼\,O_2 \qquad (1)$$

within the range $1260 < T_{dec}$, K < 1273. This allows us to evaluate T_{dec} ($YCoO_3$) = 1266 ± 6 K.

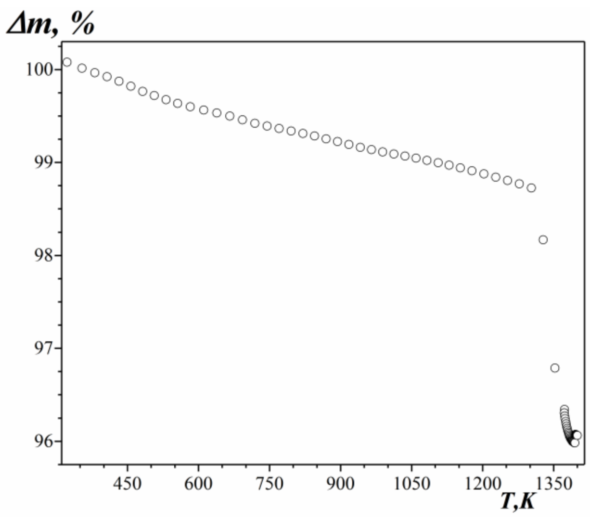

Fig. 3 TGA curve for single-phase $YCoO_3$ in air measured in a dynamic mode with a heating rate of 3.2 K/min

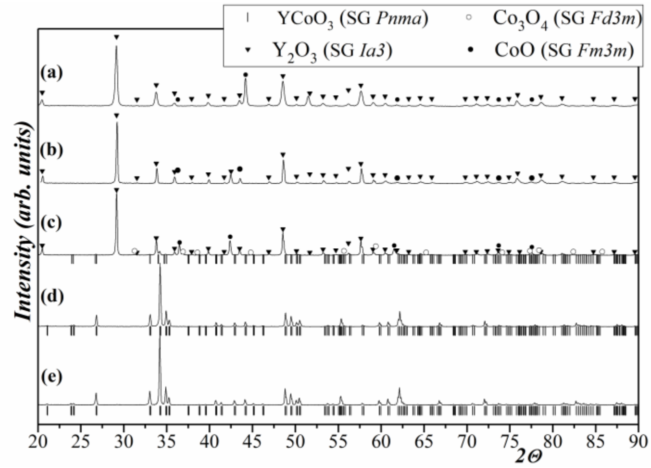

Fig. 4 XRD patterns of the samples with nominal composition of $YCoO_3$, fired and quenched from various temperatures in air: (a) 1373 K; (b) 1323 K; (c) 1273 K; (d) 1223 K; (e) 1173 K.

Prolonged annealing of the sample with nominal composition corresponding to $YCoO_3$ at 1373 K reveals coexisting of two binary simple oxides Y_2O_3 and CoO.

Since $YCoO_3$ is only stable below 1266 K, it is likely that a continuous series of $YFe_{1-x}Co_xO_3$ solid solutions cannot be obtained at higher temperatures. Indeed, continuous series of $YFe_{1-x}Co_xO_3$ solid solutions in the range of $0 \le x \le 1$ was obtained at 1173 K. The homogeneity range at 1273 K was evaluated as $0 \le x \le 0.9$. The sample with x=0.95 contained together with perovskite phase also Y_2O_3 and enriched by cobalt $Fe_{1-y}Co_yO$ with the rock salt structure (Fig. 5). Further increase of temperature leads to a decrease in Co content in the limiting $YFe_{1-x}Co_xO_3$ solid solution (Table 2).

Table 2 The homogeneity range value for the $YFe_{1-x}Co_xO_3$ solid solutions at various temperatures

T, K	homogeneity range	*T*, K	homogeneity range
1173	0≤x≤1	1373	0≤x≤0.45
1273	0≤x≤0.9	1423	0≤x≤0.3
1323	0≤x≤0.68	1473	0≤x≤0.2

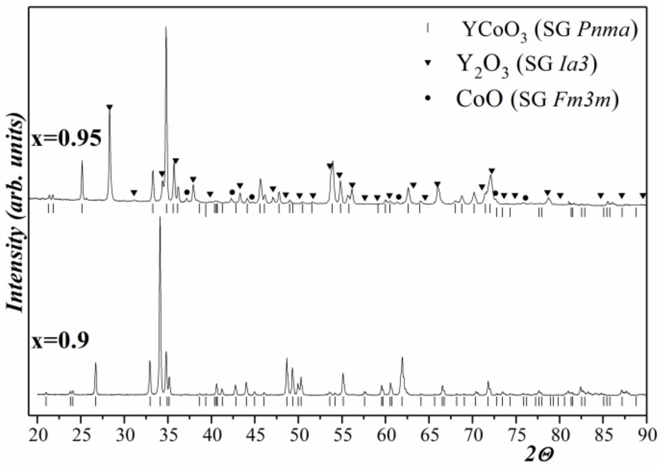

Fig. 5 XRD patterns for $YFe_{1-x}Co_xO_3$ (x=0.9, 0.95) equilibrated at 1273 K and quenched to RT

Thermal decomposition of Co-saturated solid solution with the temperature increase can be shown by following reaction:

$$YFe_{1-x'}Co_{x'}O_3 \rightarrow YFe_{1-x''}Co_{x''}O_3 + Co_{1-y'}Fe_{y'}O + Y_2O_3 + zO_2 \quad (2)$$

were $x' > x''$ and y' corresponds to the Fe-saturated solid solution at a fixed temperature. It is worth noting that the process described by scheme (2) differs significantly from the one occurs according to equation (1). The latter corresponds to a nonvariant thermodynamic equilibrium, when all participating phases coexist at fixed T and Po_2. In contrast, scheme (2) represents the situation when Co-saturated single-phase $YFe_{1-x'}Co_{x'}O_3$ solid solutions in the left-hand side exist at T', and an increase of temperature to $T'' = T' + \Delta T$ causes a depletion of cobalt in solid solution and displacement of its composition $YFe_{1-x''}Co_{x''}O_3$ as well as appearance of two secondary phases, namely, Y_2O_3 and $Co_{1-y'}Fe_{y'}O$. The left-hand side and the right-hand side in the scheme (2) represent the phase composition in the system at different temperatures, T' and $T''=T'+\Delta T$, respectively. Thus, scheme (2) describes nonequilibrium process that occurs due to the change in thermodynamic parameter, in this case it is temperature. A similar process can take place at fixed temperature due to the decrease in Po_2.

Based on the results of phase composition of all studied samples the "T-composition" phase diagram of the $YFeO_3$ – $YCoO_3$ system in air was drawn (Fig. 6).

All single-phase $YFe_{1-x}Co_xO_3$ solid solutions quenched from all studied temperatures possess the orthorhombic structure, like parent ternary oxides. The influence of temperature on the crystal structure of $YFe_{1-x}Co_xO_3$ (x = 0.35 and 0.45) was studied by *in situ* high temperature (HT) XRD measurements. The structural parameters of $YFe_{1-x}Co_xO_3$ (x = 0.35 and 0.45) at various temperatures refined by the Rietveld method are listed in Tables 3 and 4.

Temperature dependencies of the unit cell parameters and unit cell volume demonstrate visible non-linearity (Fig. 7). As a rule, the distortions of crystal structure tend to decrease with the temperature rise; however, the ortho-

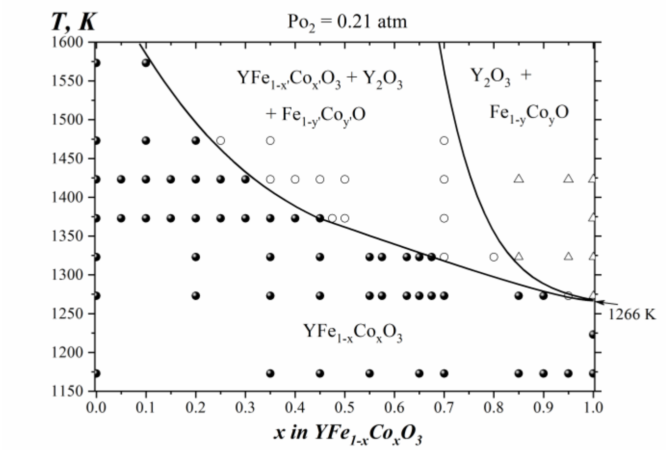

Fig. 6 Phase diagram of the $YFeO_3$ – $YCoO_3$ system in air

Table 3 The structural parameters of $YFe_{0.65}Co_{0.35}O_3$ at various temperatures refined by the Rietveld method using HT-XRD measurements

SG Pnma : Y*(4c)*(x; 0.25; z); Fe/Co*(4a)*(0; 0; 0); O1*(4c)*(x; 0.25; z); O2*(8d)*(x; y; z)							
T, K	298	473	623	673	973	1273	1373
a, Å	5.53089(6)	5.53716(4)	5.54493(4)	5.54861(4)	5.58349(4)	5.61551(6)	5.62316(5)
b, Å	7.51120(8)	7.52574(5)	7.54017(6)	7.54575(6)	7.59046(6)	7.63524(8)	7.64818(6)
c, Å	5.23159(6)	5.24225(4)	5.25323(4)	5.25755(4)	5.29060(4)	5.32228(6)	5.33169(4)
V, $(Å)^3$	217.339(4)	218.451(3)	219.636(3)	220.125(3)	224.222(3)	228.197(4)	229.300(3)
x(Y1)	0.4316(2)	0.4324(2)	0.4332(2)	0.4330(2)	0.4339(2)	0.4347(2)	0.4350(2)
z(Y1)	0.0181(3)	0.0182(3)	0.0174(3)	0.0174(3)	0.0172(3)	0.0165(3)	0.0163(3)
x(O1)	0.534(1)	0.533(1)	0.532 (1)	0.531(1)	0.533(1)	0.531(2)	0.5329(2)
z(O1)	0.603 (1)	0.605(2)	0.604(2)	0.605(2)	0.605(2)	0.606(2)	0.606(2)
x(O2)	0.196(1)	0.195(1)	0.195(1)	0.194(1)	0.193(1)	0.192(1)	0.192(1)
y(O2)	0.054(7)	0.053(7)	0.053(7)	0.053(7)	0.055(7)	0.054(7)	0.054(7)
z(O2)	0.307(1)	0.306(1)	0.307(1)	0.309(9)	0.309(1)	0.308(1)	0.307(1)
$d_{(Y)-(O1)}$, Å	2.287(7)	2.307(7)	2.314(7)	2.323(7)	2.331(7)	2.360(8)	2.371(8)
$d_{(Y)-(O2)}$, Å	2.479(5)	2.490(5)	2.503(5)	2.512(6)	2.529(6)	2.553(6)	2.557(6)
$d_{(Y)-(O2)}$, Å	2.270(5)	2.271(5)	2.272(6)	2.267(6)	2.268(6)	2.282(6)	2.287(6)
$d_{(Y)-(O2)}$, Å	2.633(5)	2.634(5)	2.635(5)	2.633(5)	2.657(6)	2.666(6)	2.672(6)
$d_{(Fe/Co)-(O1)}$, Å	1.963(2)	1.969(2)	1.971(2)	1.973(2)	1.985(2)	1.997(2)	2.002(3)
$d_{(Fe/Co)-(O2)}$, Å	1.980(5)	1.976(5)	1.982(5)	1.987(5)	2.004(6)	2.003(6)	2.004(6)
$d_{(Fe/Co)-(O2)}$, Å	2.002(5)	2.010(5)	2.012(6)	2.016(5)	2.030(6)	2.052(6)	2.056(6)
(Fe/Co)–(O1)–(Fe/Co), °	146.09(3)	146.25(2)	146.07(7)	146.00(1)	145.92(3)	145.8(2)	145.61(7)
(Fe/Co)–(O2)–(Fe/Co), °	145.91(6)	145.62(2)	145.92(2)	145.47(9)	144.92(6)	145.15(4)	145.25(7)
R_p, %	11.8	12.2	12.5	12.9	13.4	13.8	14.0
R_{wp}, %	15.0	15.2	15.2	15.7	15.8	16.0	16.2
R_{exp}, %	10.6	10.6	10.7	10.7	11.0	11.3	11.4
R_{Br}, %	4.25	4.83	4.98	4.91	5.01	5.38	5.09
R_f, %	3.43	3.87	4.05	3.89	4.26	4.80	4.91
χ^2	1.985	2.057	2.036	2.148	2.043	2.002	2.019

Table 4 The structural parameters of $YFe_{0.55}Co_{0.45}O_3$ at various temperatures refined by the Rietveld method using HT-XRD measurements

SG Pnma : Y*(4c)*(x; 0.25; z); Fe/Co*(4a)*(0; 0; 0); O1*(4c)*(x; 0.25; z); O2*(8d)*(x; y; z)						
T, K	298	623	723	873	1223	1373
a, Å	5.51229(9)	5.52600(9)	5.53528(9)	5.55559(9)	5.60219(9)	5.61552(9)
b, Å	7.48536(13)	7.51456(13)	7.52654(13)	7.54977(13)	7.60614(13)	7.62717(13)
c, Å	5.21595(9)	5.23834(9)	5.24821(9)	5.26589(9)	5.30639(9)	5.32121(8)
V, $(Å)^3$	215.218(2)	217.524(4)	218.648(7)	220.869(6)	226.111(7)	227.910(7)
x(Y1)	0.4324(3)	0.4343(3)	0.4343(3)	0.4345(3)	0.4349(3)	0.4356(3)
z(Y1)	0.0178(4)	0.0170(4)	0.0168(5)	0.0166(4)	0.0164(5)	0.0158(5)
x(O1)	0.5328(18)	0.5319(18)	0.5304(18)	0.5319(18)	0.5332(18)	0.5340(19)
z(O1)	0.6004(19)	0.5999(20)	0.5984(20)	0.6031(20)	0.6030(20)	0.602(2)
x(O2)	0.1935(15)	0.1929(15)	0.1926(15)	0.1952(15)	0.1925(15)	0.1948(16)
y(O2)	0.0547(10)	0.0530(9)	0.0524(10)	0.0527(10)	0.0538(10)	0.0541(10)
z(O2)	0.3050(15)	0.3045(15)	0.3062(15)	0.3039(15)	0.3070(15)	0.3053(16)
$d_{(Y)-(O1)}$, Å	2.25(1)	2.25 (1)	2.26(1)	2.24 (1)	2.26(1)	2.27(1)
$d_{(Y)-(O1)}$, Å	2.287(1)	2.306(1)	2.316 (1)	2.324(1)	2.338(1)	2.341(2)
$d_{(Y)-(O2)}$, Å	2.4729(8)	2.4979(8)	2.512(8)	2.505(8)	2.540(8)	2.537(9)
$d_{(Y)-(O2)}$, Å	2.250(8)	2.260(8)	2.263(8)	2.284(8)	2.278(8)	2.293(9)
$d_{(Y)-(O2)}$, Å	2.629(8)	2.630(7)	2.626(8)	2.645(8)	2.662(8)	2.678(8)
$d_{(Fe/Co)-(O1)}$, Å	1.952(3)	1.958(3)	1.959(3)	1.972(3)	1.987(3)	1.992(3)
$d_{(Fe/Co)-(O2)}$, Å	1.959(8)	1.959(8)	1.968(8)	1.974(8)	1.996(8)	2.002(9)
$d_{(Fe/Co)-(O2)}$, Å	2.014 (8)	2.022(8)	2.021(8)	2.023(8)	2.046(8)	2.0447(9)
(Fe/Co)–(O1)–(Fe/Co), °	147.017(6)	147.24(2)	147.798(6)	146.33(2)	146.222(6)	146.418(6)
(Fe/Co)–(O2)–(Fe/Co), °	145.537(6)	145.995(6)	145.861(6)	146.534(6)	145.349(6)	145.868(6)
R_p, %	15.3	15.4	15.4	15.6	15.8	16.7
R_{wp}, %	18.2	18.2	18.3	18.3	18.5	19.4
R_{exp}, %	11.7	11.5	11.5	11.6	11.9	12.3
R_{Br}, %	4.38	4.56	4.53	4.76	5.19	5.36
R_f, %	3.53	3.92	3.81	4.53	4.99	5.30
χ^2	2.429	2.503	2.528	2.471	2.398	2.481

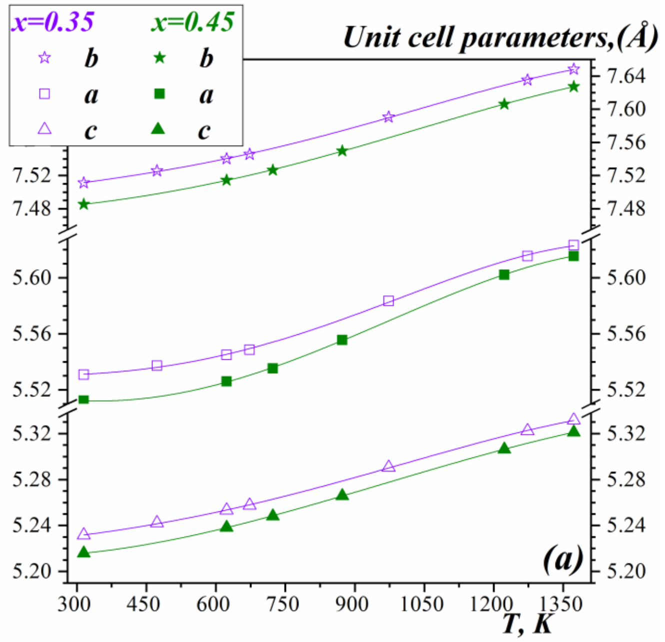

Fig. 7 The unit cell parameters and unit cell volume of $YFe_{1-x}Co_xO_3$ (x=0.35 and 0.45) versus temperature

rhombic distortion parameters calculated by the formula [26, 27]:

$$D_{orth} = \frac{1}{3}\sum_{i=1}^{3}\left|\frac{a_i - \bar{a}}{\bar{a}}\right| \times 100\% \qquad (3)$$

where D_{orth} is the orthorhombic distortion parameter, %; $\alpha_1 = a$; $\alpha_2 = b$; $\alpha_3 = c/\sqrt{2}$ and $\bar{a} = (a\times b\times c/\sqrt{2})^{1/3}$, exhibit visible anomalies within 600 – 1200 K (Fig. 8). Such behavior could not be explained by the change in oxidation states of 3d metals. TGA analysis of $YFe_{1-x}Co_xO_3$ ($x = 0.35$ and 0.45) reveals tiny mass changes while heating, which means that both oxides possess almost stoichiometric oxygen content within entire temperature range. Thus, the oxidation state of 3d atoms is equal to 3+ and remains unchanged with the increase of temperature. Another reason that can induce structural transformations can be changes in spin states. Such temperature-induced changes in the spin state of Co^{3+} ion in $LnCoO_3$ perovskites were reported by Raccach and Goodenough [28] and in later publications [7, 29-31]. Low-spin (t^6_{2g}) state can transforms into intermediate-spin ($t^5_{2g}e^1_g$) state and finally into high-spin ($t^4_{2g}e^2_g$) state. Although the possibility of spin state changes for Fe^{3+} ion is still questionable and its high-spin state is more favorable [2, 5], possible spin-state transition of Co^{3+} ion can cause the observed anomalies. However, this needs to be checked by further independent experiments.

It is worth noting that Co substitution for Fe reveals much stronger effect on changes in the unit cell volume due to the size effect ($r^{VI}_{Fe^{3+}(HS)} = 0.645$ Å, $r^{VI}_{Co^{3+}(LS)} = 0.545$ Å, $r^{VI}_{Co^{3+}(HS)} = 0.61$ Å [32]) rather than temperature. The decrease in the unit cell volume of $YFe_{1-x}Co_xO_3$ with the cobalt content (Fig. 9) is much more significant in comparison with the temperature dependence.

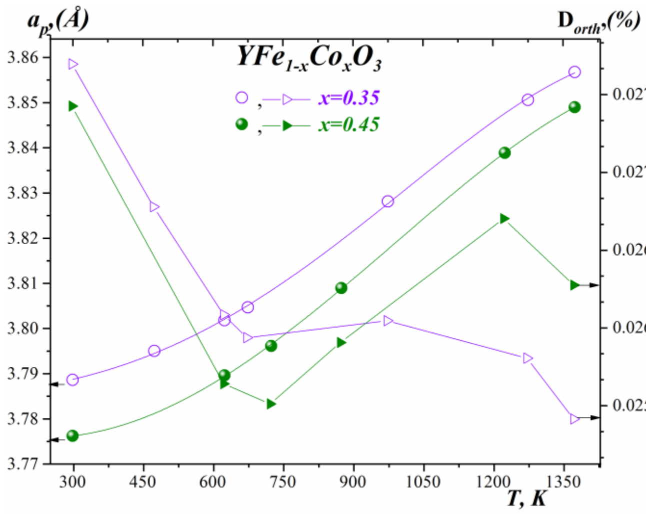

Fig. 8 The pseudo-cubic unit cell parameter (a_p) and the orthorhombic distortion parameter (D) for $YFe_{1-x}Co_xO_3$ ($x = 0.35$ and 0.45) versus temperature

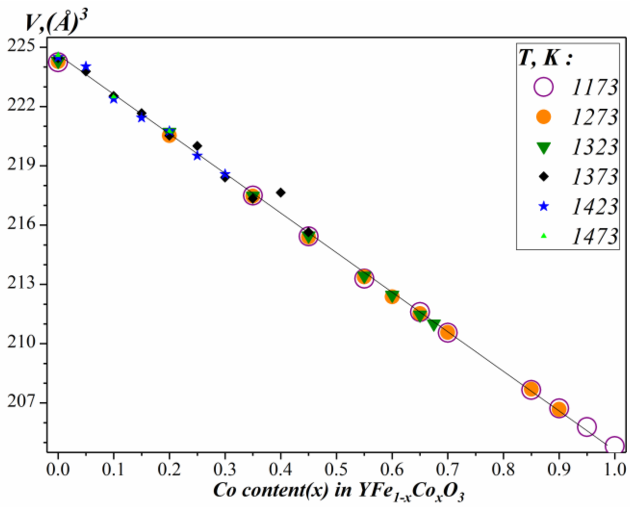

Fig. 9 The unit cell volume of $YFe_{1-x}Co_xO_3$ versus Co content (x)

4. Conclusions

The homogeneity range and crystal structure of $YFe_{1-x}Co_xO_3$ solid solution have been studied within the entire composition range (0≤x≤1) in 1173 – 1573 K temperature range. Continuous series of $YFe_{1-x}Co_xO_3$ solid solutions in air can be obtained only below decomposition temperature of $YCoO_3$, which was evaluated equal to 1266 ± 6 K. Further temperature increase leads to a decrease of $YFe_{1-x}Co_xO_3$ homogeneity range which is determined to be 0≤x≤0.1 at 1573 K. Phase diagram of the $YFeO_3$ – $YCoO_3$ system in air comprise of 3 phase fields.

Partial substitution of Co for Fe has not changed the orthorhombic perovskite structure. Possible change in the spin state of Co^{3+} ions is a presumable reason for the unusual behavior of orthorhombic distortions in $YFe_{1-x}Co_xO_3$ (x = 0.35 and 0.45) with temperature.

Acknowledgments

This work was supported in parts by the Ministry of Science and Higher Education of Russian Federation (№ AAAA-A20-120061990010-7) and A.V.B. was supported with a stipend for young scientists and PhD students from the President of Russian Federation (№ SP-3689.2019.1).

References

1. Rosales-González O, Sánchez-De Jesús F, Cortés-Escobedo CA, Bolarín-Miró AM. Crystal structure and multiferroic behavior of perovskite $YFeO_3$. Ceram Int. 2018; 4:15298-303. doi:10.1016/j.ceramint.2018.05.175
2. Cheng ZX, Shen H, Xu JY, Liu P, Zhang SJ. Magnetocapacitance effect in nonmultiferroic $YFeO_3$ single crystal. J Appl Phys. 2012;111:034103-1–5. doi:10.1063/1.3681294
3. Zhang Y, Yang J, Xu J, Gao Q, Hong Z. Controllable synthesis of hexagonal and orthorhombic $YFeO_3$ and their visible-light photocatalytic activity. Mater Lett. 2012;81:1–4. doi:10.1016/j.matlet.2012.04.080
4. Maiti R, Basu S, Chakravorty D. Synthesis of nanocrystallineYFeO_3 and its magnetic properties. J Magn Magn Mater. 2009;321:3274–7. doi:10.1016/j.jmmm.2009.05.061
5. Lin X, Jiang J, Jin Z, Wang D, Tian Z, Han J, Cheng Z, Ma G. Terahertz probes of magnetic field induced spin reorientation in $YFeO_3$ single crystal. Appl Phys Lett. 2015;106:092403-1–4. doi:10.1063/1.4913998
6. Addabbo T, Bertocci F, Fort A, Mugnaini M, Shahin L, Vignoli V, Spinicci R, Rocchi S, Gregorkiewitz M. An artificial olfactory system (AOS) for detection of highly toxic gases in air based on $YCoO_3$. Procedia Eng. 2014;87:1095–8. doi:10.1016/j.proeng.2014.11.355
7. Knížek K, Jirák Z, Hejtmánek J, Veverka M, Maryško M, Maris G, Palstra TTM. Structural anomalies associated with the electronic and spin transitions in $LnCoO_3$. Eur Phys J B. 2005:47:213–20. doi:10.1140/epjb/e2005-00320-3
8. Zhu Z, Guo J, Jia Y, Hu X. Electronic structure and evolution of spin state in $YCoO_3$. Phys B. 2010;405:359–62. doi:10.1016/j.physb.2009.08.097
9. Knizek K, Jirak Z, Hejtmanek J, Veverka M, Marysko M, Hauback BC, Fjellvag H. Structure and physical properties of $YCoO_{3-\delta}$ at temperatures up to 1000 K. Phys Rev B: Condens Matter Mater Phys. 2006;73:214443. doi:10.1103/PhysRevB.73.214443
10. Krén E, Pardavi M, Pokó Z, Sváb E, Zsoldos É. Study of the Spin Reorientation in Co- and Cr-Substituted YFeO3. AIP Conf Proc 10. 1973;10:1603–6. doi:10.1063/1.2946858
11. Pomiro F, Gil DM, Nassif V, Paesano AJr, Gómez MI, Guimpel J, Sánchez RD, Carbonio RE. Weak ferromagnetism and superparamagnetic clusters coexistence in $YFe_{1-x}Co_xO_3$ (0≤x≤1) perovskites. Mater Res Bull. 2017;94:472-82. doi:10.1016/j.materresbull.2017.06.045
12. Wei Y, Gui H, Zhao Z, Li J, Liu Y, Xin S, Li X, Xie W. Structure and magnetic properties of the perovskite $YCo_{0.5}Fe_{0.5}O_3$. AIP Adv. 2014;4:127134. doi:10.1063/1.4904811
13. Imitrovska-Lazova S, Aleksovska S, Tzvetkov P. Synthesis and crystal structure determination of $YCo_{1-x}Fe_xO_3$ (x = 0, 0.33, 0.5, 0.67 and 1) perovskites. J Chem Sci. 2015;127(7):1173–81. doi:10.1007/s12039-015-0878-y
14. Geller S, Wood EA. Crystallographic studies of perovskite-like compounds. I. Rare earth orthoferrites and $YFeO_3$, $YCrO_3$, $YAlO_3$. Acta Cryst. 1956;9:563-8. doi:10.1107/S0365110X56001571
15. Buassi-Monroy OS, Luhrs CC, Chávez-Chávez A, Michel CR. Synthesis of crystalline $YCoO_3$ perovskite via sol–gel method. Mater Lett. 2004;58:716–8. doi:10.1016/j.matlet.2003.07.001
16. Feng G, Xue Y, Shen H, Feng S, Li L, Zhou J, Yang H, Xu D. Sol–gel synthesis, solid sintering, and thermal stability of single-phase $YCoO_3$. Phys Status Solidi A. 2012;209(7):1219–24. doi:10.1002/pssa.201127710
17. Kimizuka N, Katsura T, Standard free energy of formation of YFeO, $Y_3Fe_5O_{12}$, and a new compound YFeO in the Fe-FeO-Y_2O_3 system at 1200°C. J Solid State Chem. 1975;13:176-81. doi:10.1016/0022-4596(75)90116-4
18. Kitayama K, Sakaguchi M, Takahara Y, Endo H, Ueki H. Phase equilibrium in the system Y–Fe–O at 1100°C. J Solid State Chem. 2004;177:1933–8. doi:10.1016/j.jssc.2003.12.040
19. Piekarczyk W, Weppner W, Rabenau A. Dissociation pressure and Gibbs energy of formation of $Y_3Fe_5O_{12}$ and $YFeO_3$. Mater Res Bull. 1978;13:1077-83. doi:10.1016/0025-5408(78)90174-5
20. Tretyakov YuD, Kaul AR, Portnoy VK. Formation of rare earth and yttrium orthferrites: a thermodynamic study. High Temp Sci. 1977;9:61-70.
21. Jacob KT, Rajitha G. Nonstoichiometry, defects and thermodynamic properties of $YFeO_3$, YFe_2O_4 and $Y_3Fe_5O_{12}$. Solid State Ionics. 2012;224:32-40. doi:10.1016/j.ssi.2012.07.003
22. Masse DP, MUAN A. Phase Equilibria at Liquidus Temperatures in the System Cobalt Oxide-Iron Oxide-Silica in Air. J Am Ceram Soc. 1965;48:466-9. doi:10.1111/j.1151-2916.1965.tb14800.x
23. Zhang WW, Chen M. Thermodynamic modeling of the Co–Fe–O system. CALPHAD. 2013;41:76-88. doi:10.1016/j.calphad.2013.02.002
24. Jung I-H, Decterov SA, Pelton AD, Kim H-M, Kang Y-B. Thermodynamic evaluation and modeling of the Fe–Co–O system. Acta Mater. 2004;52:507–519. doi:10.1016/j.actamat.2003.09.034
25. Jadhao VG, Singru RM, Rama Rao G, Bahadur D, Rao CNR. Effect of the Rare Earth Ion on the Spin State Equilibria in Perovskite Rare Earth Metal Cobaltates. Yttrium trioxocobaltate(III) and erbium trioxocobaltate(III). J Chem Soc, Faraday Trans 2. 1975;71:1885–93. doi:10.1039/F29757101885
26. Ahmad I, Akhtar MJ, Siddique M, Iqbal M, Hasan MM. Origin of anomalous octahedral distortions and collapse of magnetic ordering in $Nd_{1-x}Sr_xFeO_3$ (0≤x≤0.5). Ceram Int. 2013;39:8901–9. doi:10.1016/j.ceramint.2013.04.084
27. Dasgupta N, Krishnamoorthy R, Jacob KT. Crystal structure and thermal and electrical properties of the perovskite solid solution $Nd_{1-x}Sr_xFeO_{3-\delta}$ (0≤x≤0.4). Solid State Ionics. 2002;149:227–36. doi:10.1016/S0167-2738(02)00179-0
28. Raccach PM, Goodenough JB. A localized-electron collective-electron transition in the system (La, Sr)CoO_3. J Appl Phys. 1968;39(2):1209-10. doi:10.1063/1.1656227

29. Yan J-Q, Zhou J-S, Goodenough JB. Bond-length fluctuations and the spin-state transition in $LCoO_3$ (L=La, Pr, and Nd). Phys Rev B. 2004;69:134409-1–6. doi:10.1103/PhysRevB.69.134409
30. Zhou J-S, Yan J-Q, Goodenough JB. Bulk modulus anomaly in $RCoO_3$ (R=La, Pr, and Nd). Phys. Rev. B. 2005;71:220103-1–4. doi:10.1103/PhysRevB.71.220103
31. Cavalcante FHM, Carbonari AW, Malavasi RFL, Cabrera-Pasca GA, Saxena RN, Mestnik-Filho J. Investigation of spin transition in $GdCoO_3$ by measuring the electric field gradient at Co sites. J Magn Magn Mater. 2008;320:e32–5. doi:10.1016/j.jmmm.2008.02.033
32. Shannon RD. Revised effective ionic radii and systematic studies of interatomic distances in halides and chalcogenides. Acta Crystallogr, Sect A. 1976; 32(5):751–67. doi:10.1107/s0567739476001551